1-1-2014

Investigation of ultrafine grained AA1050 fabricated by accumulative roll bonding

Lihong Su
University of Wollongong, lihongsu@uow.edu.au

Cheng Lu
University of Wollongong, chenglu@uow.edu.au

Huijun Li
University of Wollongong, huijun@uow.edu.au

Guanyu Deng
University of Wollongong, gdeng@uow.edu.au

A Kiet Tieu
University of Wollongong, ktieu@uow.edu.au

Investigation of ultrafine grained AA1050 fabricated by accumulative roll bonding

Abstract

Accumulative roll bonding (ARB) is an effective method to produce ultrafine-grained (UFG) sheet materials with high strength. In this work, fully annealed AA1050 sheet with an initial thickness of 1.5. mm was processed by ARB up to five cycles. The microstructure was examined by optical microscopy (OM) and transmission electron microscopy (TEM). The results revealed that ARB is a promising process for fabricating ultrafine grained structures in aluminium sheets and the average grain size after 5-cycle ARB reached approximately 300. nm. Meanwhile, a remarkable enhancement in the strength was achieved and the value was about three times the strength of starting material. The microstructure at the bond interface introduced during ARB was investigated and its influence was discussed in detail. In addition, the microstructure and mechanical properties after ARB were compared with that after deformation by equal channel angular pressing (ECAP) up to the same strain. It has been found that ARB is more efficient in grain refinement and strengthening, which can be attributed to the different deformation modes of the two techniques.

Keywords

grained, aa1050, fabricated, accumulative, investigation, roll, ultrafine, bonding

Disciplines

Engineering | Science and Technology Studies

Publication Details

Su, L., Lu, C., Li, H., Deng, G. & Tieu, K. (2014). Investigation of ultrafine grained AA1050 fabricated by accumulative roll bonding. Journal of Materials Science and Engineering A, 614 148-155.

Materials Science & Engineering A 614 (2014) 148–155

Contents lists available at ScienceDirect

Materials Science & Engineering A

journal homepage: www.elsevier.com/locate/msea

Investigation of ultrafine grained AA1050 fabricated by accumulative roll bonding

Lihong Su, Cheng Lu*, Huijun Li, Guanyu Deng, Kiet Tieu

School of Mechanical, Materials and Mechatronic Engineering, University of Wollongong, Wollongong, NSW 2522, Australia

ARTICLE INFO

Article history:
Received 25 March 2014
Received in revised form
1 July 2014
Accepted 12 July 2014
Available online 19 July 2014

Keywords:
Accumulative roll bonding
Aluminium alloy
Microstructure
Strength
Microhardness
Bond interface

ABSTRACT

Accumulative roll bonding (ARB) is an effective method to produce ultrafine-grained (UFG) sheet materials with high strength. In this work, fully annealed AA1050 sheet with an initial thickness of 1.5 mm was processed by ARB up to five cycles. The microstructure was examined by optical microscopy (OM) and transmission electron microscopy (TEM). The results revealed that ARB is a promising process for fabricating ultrafine grained structures in aluminium sheets and the average grain size after 5-cycle ARB reached approximately 300 nm. Meanwhile, a remarkable enhancement in the strength was achieved and the value was about three times the strength of starting material. The microstructure at the bond interface introduced during ARB was investigated and its influence was discussed in detail. In addition, the microstructure and mechanical properties after ARB were compared with that after deformation by equal channel angular pressing (ECAP) up to the same strain. It has been found that ARB is more efficient in grain refinement and strengthening, which can be attributed to the different deformation modes of the two techniques.

1. Introduction

Over years, efforts have been made by researchers around the world in order to produce materials with submicron or even nanosized grains, since the average grain size plays a significant role on the mechanical properties of crystalline materials. According to the well-known Hall–Petch equation, the strength increases with a reduction in the grain size [1]. Therefore, fabricating materials with a grain size in the nano-range (less than 100 nm) or ultrafine range (between 100 nm and 1 μm) is an effective approach to increase the strength of materials [2].

It is well known that heavy deformation, such as cold rolling, can result in microstructure refinement. However, as there are always limits in the total strain that can be imposed on the materials, the structures formed are usually subgrains with low angle grain boundaries [3]. Severe plastic deformation (SPD), on the other hand, can produce materials with refined grains separated by many high angle grain boundaries, through imposing large amount of plastic strain on the materials as the external dimensions of the samples are designed to be kept unchanging during different passes. Using SPD techniques to process ultrafine grained (UFG) materials from coarse grained metals and alloys has attracted much attention since more than 30 years ago [3].

Up to now, a number of different SPD processing techniques have been developed, such as equal channel angular pressing (ECAP) [3], high pressure torsion (HPT) [4] and accumulative roll bonding (ARB) [5]. Among these processes, ECAP and ARB are two of the most frequently used SPD techniques. ARB was first introduced by Saito et al. [5] and is considered to be one of the most promising methods for manufacturing UFG sheet materials [6–8]. The ARB process is shown schematically in Fig. 1. During ARB, rolling is conducted on two sheets with the same dimension which have been stacked together beforehand. The rolling process not only provides large plastic deformation but also bonds the two sheets together. The bonded specimen of each cycle is prepared by cutting, surface degreasing, brushing, and stacking together for the next cycle [5,6]. The reduction in thickness after each pass is approximately 50% and the increase in width is negligible, thus the thickness of the bonded materials should remain the same during the whole rolling process. Since in theory the number of repetitions is endless, it is possible to achieve ultrahigh strain with the ARB process.

During ARB, the sample is assumed to be deformed in a plain strain condition. Therefore, the equivalent strain ε_{eq}, can be calculated using the following equation [6]:

$$\overline{\varepsilon}_{eq} = \frac{2}{\sqrt{3}} n \ln \frac{h_0}{h} = \frac{2}{\sqrt{3}} n \ln \frac{1}{1-r} \quad (1)$$

where h_0 is the initial thickness of the stacked sheets, h is the thickness after roll-bonding, r is the reduction in thickness per cycle and n is the number of ARB cycles. The reduction per ARB

* Corresponding author. Tel.: +61 2 42214639.
E-mail address: chenglu@uow.edu.au (C. Lu).

http://dx.doi.org/10.1016/j.msea.2014.07.032
0921-5093/

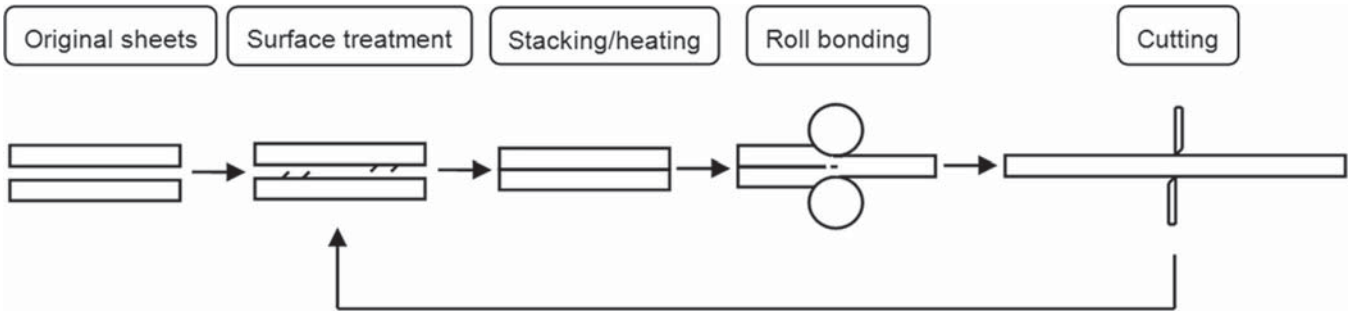

Fig. 1. Schematic illustration of the ARB process.

cycle is usually $r = 50\%$, which results in an equivalent strain of about 0.8/cycle.

Aluminium and its alloys have great potential in automotive and aerospace industry applications due to their light-weight nature, good formability, good corrosion resistance and low cost [9–11]. However, the application is limited mostly due to their low strength compared with other metallic materials like steels. Using SPD techniques to improve the strength of aluminium and its alloys can expand their usage in these industries. Many aluminium based alloys have been processed by ARB in the literature. For commercial purity aluminium, for example, Huang et al. carried out ARB of AA1100 at 473 K and they found that the microstructure after two cycles was composed of sub-micrometer lamellar structures [12]. Pirgazi et al. succeeded to conduct ARB of AA1100 up to 10 cycles at the same deformation temperature [13]. Kwan et al. reported on the subsequent annealing of ARB processed AA1100 and their results indicated a rapid grain growth when the annealing temperature was higher than 150 °C. Li et al. [14] studied the texture evolution during ARB of AA1070 and strong texture gradients were observed. Besides, Quadir et al. [15] and Jamaati et al. [16,17] have investigated the influence of rolling reduction varying from 20% to 90% on the bond strength during ARB. It was found that the bond strength increased significantly for reductions greater than 47%. The formability and wear characteristics after ARB have also been studied in [18] and [19], respectively. However, most of these reports were only focused on the evolution of a particular property after ARB deformation. A systematic study on the properties of the ARB processed commercial pure aluminium is still essential, and some aspects of the properties like the interfacial microstructure and its formation mechanism and effects have never been studied in detail. Böhner et al. [20] studied the difference of commercial purity aluminium after ECAP and ARB to the same strain by the tensile test and nanoindentation and found that the material after ARB was stronger at the tensile test but weaker at the nanoindentation test. The difference in microstructure was not studied.

In this work, AA1050 sheets were processed by ARB and the evolution of microstructure and mechanical properties was examined. The microstructure at the bond interface was investigated and discussed in detail particularly and the comparison of the microstructure and mechanical properties of AA1050 after ARB and ECAP to the same accumulated strain was also made.

2. Experimental procedure

AA1050 sheets were produced by ARB using annealed AA1050 sheets as the starting materials. Two pieces of aluminium sheets were stacked and welded together at one end, pre-heated in a furnace at 200 °C for 3 min and then rolled with a rolling mill consisting of 125 mm diameter rolls and kept at room temperature. The true rolling temperature was above room temperature but less than 200 °C. The rolling was conducted with a nominal reduction of 50% under dry condition. The rolled samples were cut into two halves and stacked together again to perform the next cycle. The above procedure proceeded for 5 cycles to achieve an accumulative strain of about 4.

The mechanical properties were tested by tensile and hardness tests. The hardness measurement was taken using a load of 25 g and a dwell time of 12 s. The measurement was taken on the rolling direction (RD)–normal direction (ND) plane along the thickness direction with 50 μm distance of two adjacent indents. Through-thickness hardness distributions and average hardness values were obtained. Tensile specimens with a 25 mm gauge length and a 6 mm gauge width were processed with the longitudinal direction parallel to the rolling direction of the ARB processed samples. Tensile tests were conducted at ambient temperature and with an initial strain rate of 10^{-3}/s.

Optical microscopy was conducted on a Leica DMRM microscope. The samples were prepared by grinding and polishing to an OPS finish and then etching with Barker's reagent. The microstructure images were taken on the longitudinal cross-section (RD–ND plane) for the annealed and ARB processed samples. Transmission electron microscopy (TEM) micrographs were obtained with a JEOL 2011F microscope operating at 200 kV. Thin foils for TEM were prepared by twin-jet electron polishing with an electrolyte of 25% nitric acid in methanol at −20 °C. Scanning electron microscopy (SEM) images were taken with a JEOL 6490 microscope.

3. Results

3.1. Evolution of microstructure

Fig. 2 shows the optical microstructure of the AA1050 samples before and after ARB. All the optical micrographs were taken on the RD–ND plane close to the thickness centre. The AA1050 sheets before ARB had a fully annealed homogeneous microstructure, as shown in Fig. 2(a). The average grain size is 96 μm. After 1-cycle ARB, the grain thickness reduces and the grains are strongly elongated along the rolling direction, as can be seen in Fig. 2(b). The grain reduction after 3-cycle ARB is substantial and after 5-cycle ARB, the grain thickness further reduces but is not as considerable, at least in the optical resolution. However, the misorientation between the grains seems to be larger and the aspect ratio appears to be smaller, as can be seen in Fig. 2(d).

Fig. 3 shows the TEM micrographs after 1, 3 and 5-cycle ARB processing. The microstructure of AA1050 after 1-cycle ARB comprises slightly elongated subgrains and dense dislocation cells. The grains after 3 and 5-cycle ARB are still slightly elongated and are aligned along a certain direction, but the grain boundaries are more clearly defined. Most of the grains are clearly defined with high angle boundaries after 5-cycle ARB, while some grains involved a high density of dislocations at the grain interiors. This

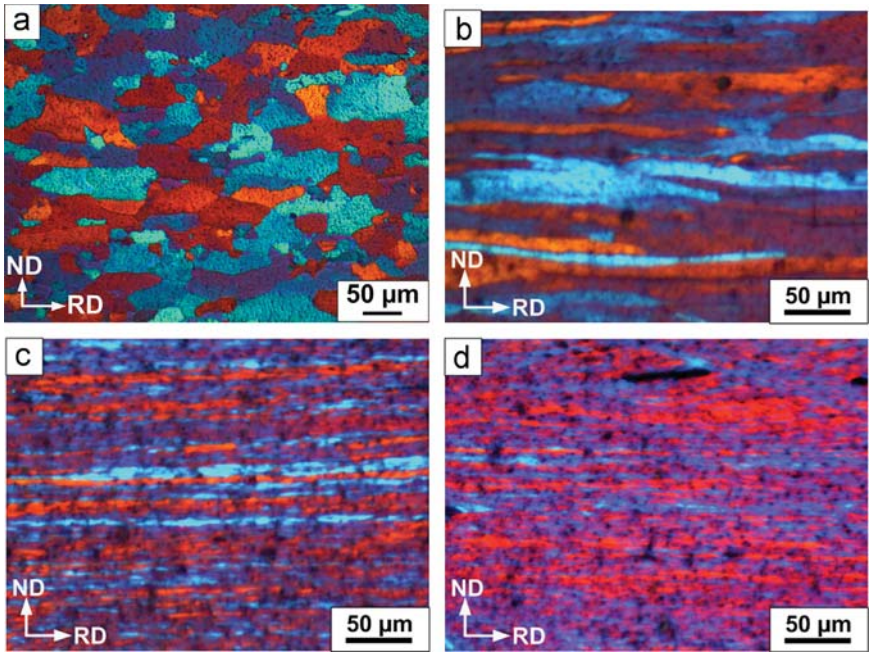

Fig. 2. Optical micrographs of AA1050 (a) before ARB and after (b) 1, (c) 3 and (d) 5-cycle ARB processing.

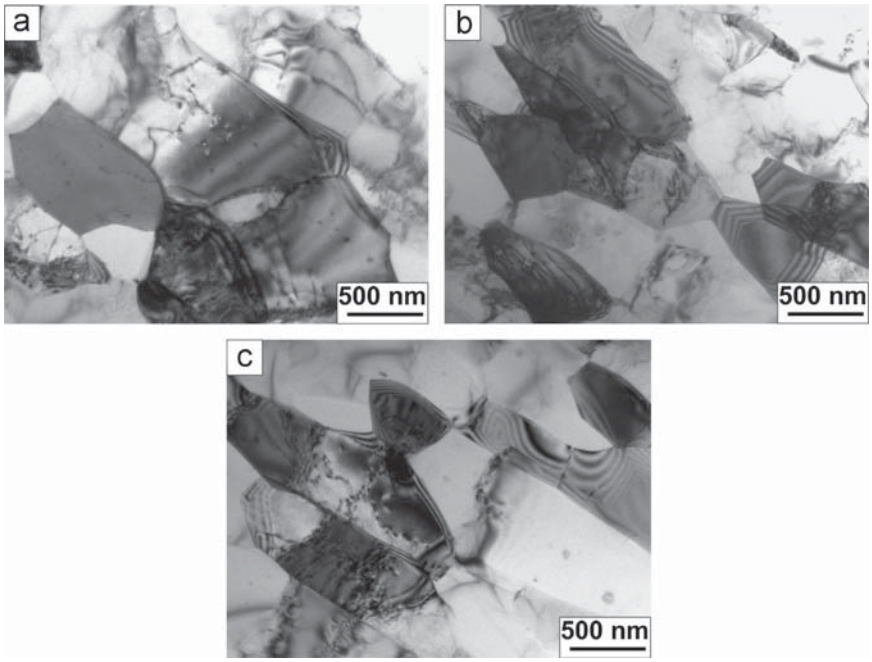

Fig. 3. TEM micrographs of AA1050 after (a) 1, (b) 3 and (c) 5-cycle ARB processing.

is the typical microstructure of ARB processed commercial purity aluminium [12,21]. The grain sizes of the 1, 3 and 5-cycle ARB processed AA1050 sheets measured from TEM micrographs are approximately 465 nm, 406 nm and 300 nm, respectively.

Fig. 4 shows the TEM micrographs close to the bond interfaces of the ARB processed AA1050. For the material after 1-cycle ARB, the microstructure close to the bond interface appears to be similar to that in the bulk (Fig. 4(a)). There is a bright line along the interface which was formed during twin-jet polishing. The microstructures close to the interfaces of the 5-cycle ARB processed AA1050 have several different types. Fig. 4(b) shows a type of microstructure which is similar to Fig. 4(a). Fig. 4(c) shows a narrow band of much more refined grains at the interface. The contrast of the narrow band is similar to that of the bulk metal. In Fig. 4(d), much more refined grains can also be seen at the interface, but the band width is wider than that in Fig. 4(c) and there is a crack along the middle of the refined band.

3.2. Evolution of mechanical properties

The average hardness evolution of AA1050 sheets with the number of ARB cycles is shown in Fig. 5(a). The annealed AA1050 has a hardness of ~29 before deformation and the hardness increases considerably after 1-cycle ARB by a factor of approximately 2 and increases further with subsequent ARB cycles, but at a lower rate. This increment continues up to 5-cycle ARB deformation without saturation, as reported for many materials, which is due to pre-heating before ARB [18].

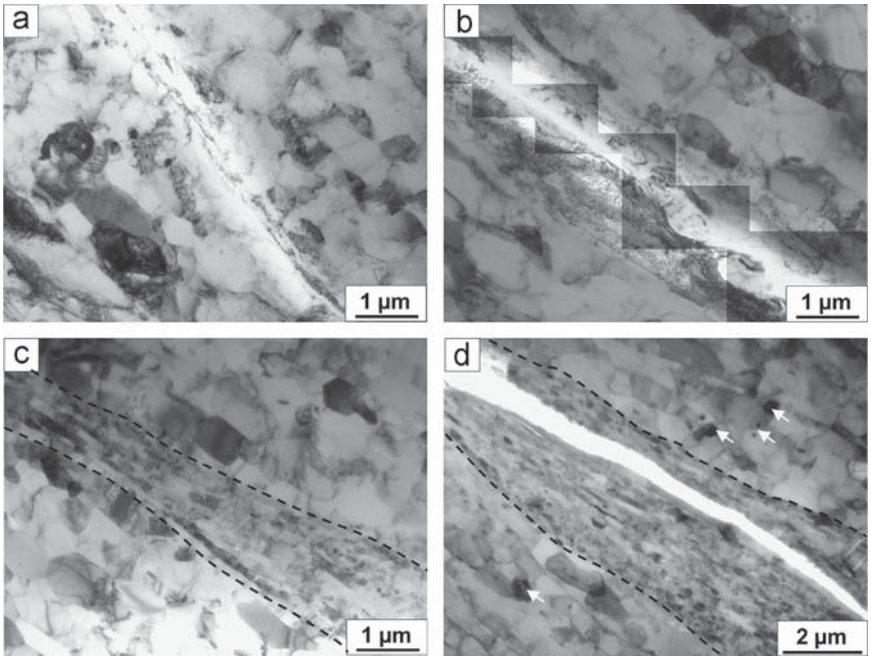

Fig. 4. TEM micrographs showing the bond interfaces of AA1050 after (a) 1, and (b)–(d) 5-cycle ARB processing.

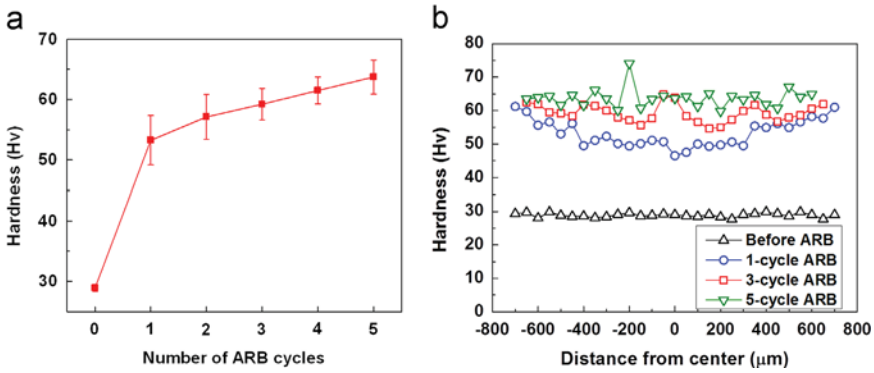

Fig. 5. (a) Average hardness of 1–5-cycle ARB processed AA1050 and (b) through-thickness hardness distribution of 1, 3 and 5-cycle ARB processed AA1050.

Fig. 5(b) shows the through-thickness hardness distribution before and after 1, 3 and 5-cycle ARB processed AA1050 sheets. The hardness along the thickness direction shows a constant value before ARB. After 1-cycle ARB, the hardness has the lowest values around the centre of the sheet and gradually increases towards the surface. After 3-cycle ARB, the hardness values are higher near the surface and the interfaces formed at the second and third ARB cycles. The hardness distribution after 5-cycle ARB is not uniform and it is difficult to see obvious high and low values regions.

Tensile test results of AA1050 sheets before and after 1–5-cycle ARB deformation are shown in Fig. 6. The engineering stress–strain curves (Fig. 6(a)) show that the stress increases and the elongation decreases after ARB deformation. Similar trends have also been observed in the ARB processed aluminium [13,22] and other materials [23]. The average values of ultimate tensile strength (UTS) and uniform elongation of the ARB processed AA1050 sheets are shown in Fig. 6(b). These values were calculated by averaging over three samples. The figure shows that after 1-cycle of ARB, the UTS of the sheet is about 172 MPa, which is about twice the strength of AA1050 before ARB deformation (85 MPa). The tensile strength increases with the number of ARB cycles from the second to the fifth cycle ARB, although at a slower rate. The value increases up to 243 MPa after 5-cycle ARB, which is about three times the initial value of the starting material. This indicates that the materials are efficiently strengthened by ARB deformation. The uniform elongation after 1-cycle ARB is about 1.5%, which drops substantially compared to the original material and then stays about the same with further ARB cycles.

Fig. 6(c) shows the effect of ARB deformation on the strain hardening rate, which is plotted against the true strain. It can be seen that the strain hardening rate of the ARB processed AA1050 is higher than the original annealed material at low true strain but it decreases rapidly at a very early stage. For the initial annealed materials, on the other hand, the strain hardening rate remains at a relative high value even at a strain as high as 30%. For the ARB processed AA1050, the strain hardening rate increases with the number of ARB cycles.

Fig. 7 shows the fracture graphs of ARB processed AA1050 after the tensile test. It shows shear zones and dimples, which are characteristics of ductile fracture. These results are consistent with the observations in Ref. [24]. As can be seen in Fig. 7(a)–(c), more necking occurs for 1 and 3-cycle ARB processed AA1050 than that after 5-cycle ARB. Delamination at the bond interfaces can be observed for all the fracture surfaces. It can be seen that the bond interface of AA1050 after 1-cycle ARB (Fig. 7(a)) is quite obvious after tensile fracture. The materials close to the interface appears to have experienced the similar shear deformation to that close to both surfaces. After 3-cycle ARB, the bond interfaces formed at the

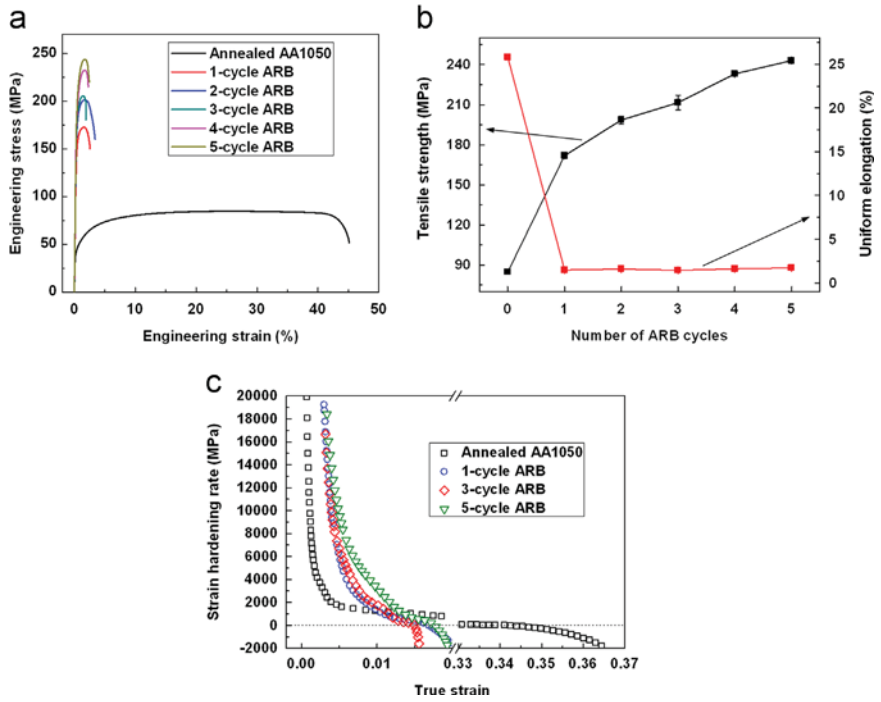

Fig. 6. (a) Engineering stress–strain curves and (b) tensile strength and uniform elongation of 1–5-cycle ARB processed AA1050, and (c) strain hardening rate of AA1050 before and after 1, 3 and 5-cycle ARB processing.

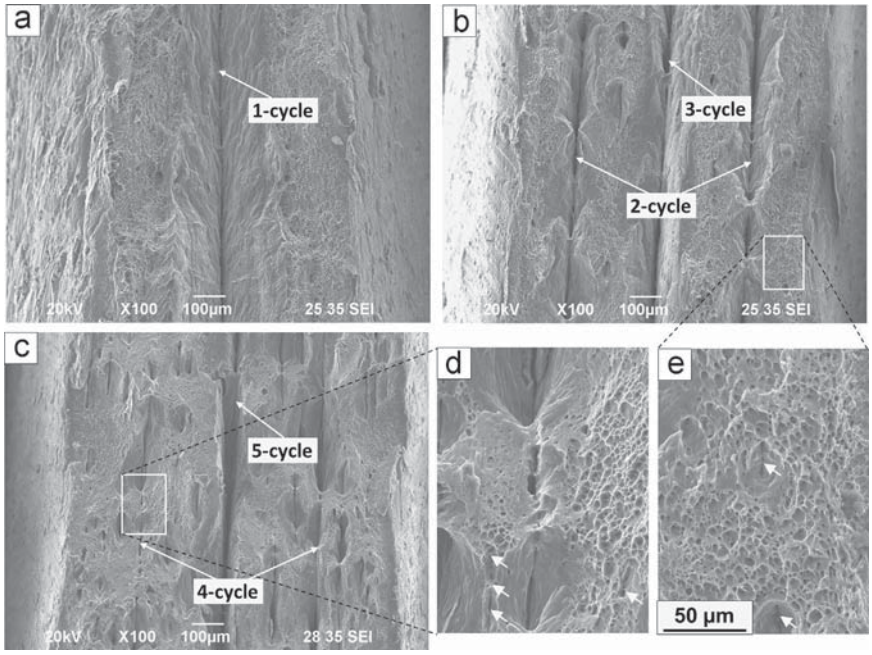

Fig. 7. Tensile fractured surfaces of AA1050 after (a) 1, (b) 3 and (c) 5-cycle ARB processing; (d) and (e) enlargements of the regions in the white frame of (c) and (b), respectively.

second and the third cycle ARB are very clear and deep (Fig. 7(b)). Those interfaces formed at the first cycle ARB, on the other hand, become invisible at most of the locations. As can be seen in the enlarged image shown in Fig. 7(e), very few delamination spots can be observed along the bond interface formed at the first cycle ARB and their sizes are quite small, as indicated by the white arrows. The fracture surface of the AA1050 after 5-cycle ARB shows deep delamination at the interfaces formed at the fourth and fifth cycle ARB (Fig. 7(c)). The interfaces formed at the second and the third cycles are still visible at low magnification but they become shallow and discontinuous compared to the fracture surface after 3-cycle ARB. The interfaces formed at the first cycle ARB are almost invisible even at high magnification (Fig. 7(d), indicated by white arrows).

4. Discussion

4.1. Bond interface

It is well known that ARB is a solid phase welding process. In Ref. [25], mechanisms of cold weld bonding were concluded to be

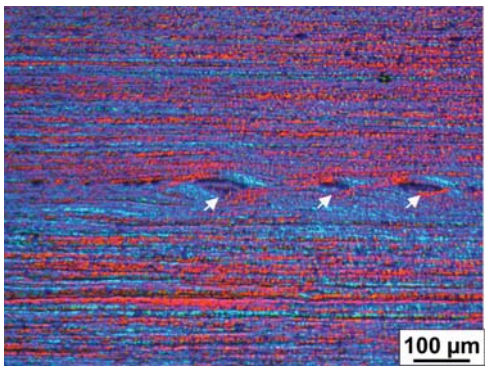

Fig. 8. Optical micrograph showing a bond interface after 3-cycle ARB.

fracture of brittle cover layer formed by scratch-brushing and contaminant film of oxides and water vapour followed by extrusion of base material through the cracks and then build-up of real contact and coalescence with base material from the opposite surface. The broken brittle surface layer was described as "pearls on a string" and the similar morphology can also be observed in the current study, as shown in Fig. 8.

It can be seen in Fig. 4 that there are basically two types of interfacial microstructures: the ones with more refined microstructure at the interfaces and the ones without. The more refined microstructure is caused by the oxides and contamination at the surfaces where the interfaces had been introduced in the previous ARB cycles [11,15,26]. The similar interfacial microstructure was been observed in the authors' previous work and was concluded as two types: type I with direct contact of fresh metals and type II with oxide film layers in between of original metal surface [26]. These two types of interfaces also apply in the current experiment, with Fig. 4(a) and (b) being type I and Fig. 4(c) and (d) being type II.

However, there are some differences in the interfacial microstructure observed in the current study and that observed in Ref. [26]. The contrast of the interfacial area is similar to that of the bulk metal for all the cases in Ref. [26], which indicates that the interface is as strong as the bulk metal during twin-jet polishing. By contrast, in the current study, the interfacial area for the type I interface shows as a bright line (Fig. 4(a) and (b)), indicating the interfaces are weak compared to the bulk metal. Fig. 4(c) shows a similar interfacial microstructure to Fig. 2(d) in Ref. [26] and Fig. 10 in Ref. [11], which seems to be as strong as the bulk. Fig. 4 (d) shows a different interfacial microstructure from all those reported in the literature, with a crack in the middle of the refined microstructure, which may occur during the twin-jet polishing stage or because the two pieces of metals were not bonded at all. This type of interfacial microstructure is more likely from the region indicated by white arrows in Fig. 8.

The interfacial microstructure has an influence on the bond strength. The more refined microstructure at the interfaces is considered to be able to improve the bond strength by increasing the hardness values close to the interfaces [15,27]. The current results are consistent with this statement as higher values are observed close to the interfacial areas (Fig. 5(b)). However, it cannot be concluded that all kinds of refined microstructure at the interfaces have positive effects on improving the bond strength. When the band width of the more refined grains exceeds a certain level or large particles or contamination gets into the sample (indicated by white arrows in Fig. 4(d)), the interfaces may act as origins of cracks, such as the image shown in Fig. 4(d).

As can be seen in Fig. 7, severe delamination along the interfaces happens during tensile tests and most of the interfaces show partly well-bonded areas and partly delaminated areas. This phenomenon also proves that there are two types of interfaces in the ARB deformed AA1050. The well-bonded areas are most probably the interfaces with thin layer of more refined microstructure (Fig. 4(c)) while the delaminated areas may be the interfaces with direct metal contact (Fig. 4(a) and (b)) or with wide bands of more refined grains (Fig. 4 (d)). The bonding quality is affected by many parameters, such as rolling temperature, amount of deformation and post-rolling annealing [15,28]. For the AA1050 after different numbers of ARB cycles, the amount of deformation increases and the bonding quality improves. As can be seen in Fig. 7, the delamination of the interfaces formed at the first cycle ARB significantly reduces after 3 and 5-cycle ARB deformations, because additional strain improves the bonding quality.

4.2. Mechanical properties

The hardness along the thickness direction of AA1050 after 1-cycle ARB has the lowest values around the centre of the sheet and gradually increases towards the surface (Fig. 5(b)). This behaviour was observed previously and was explained by more refined microstructure caused by the redundant shear strain near the surface [11]. The hardness after 3-cycle ARB has high values close to the surfaces and the interfaces formed at the second and the third cycle ARB. The higher hardness close to the surfaces is due to the redundant shear strain caused by friction between the sheet and the rolls, and the higher hardness close to the layer interfaces is due to the more refined microstructure at the interfaces and the redundant strain from the previous cycle. The interfaces formed at a particular ARB cycle were at the surfaces in the previous cycles, where enormous shear strain induced by high friction between the surfaces of AA1050 sheet and rolls was accumulated before they were deformed at the centre to form a new interface. Therefore, the hardness shows higher values close to the interfaces. In addition, the existence of oxide particles along the bonding interface and the wire brushing process before ARB can also lead to high value of hardness [11]. For the 5-cycle ARB processed AA1050, the average hardness further increases as the microstructure further refines, thus the hardness distribution becomes more random and no obvious difference can be observed at the surfaces and the interfaces. The hardness distribution through the thickness in the current work is similar to the authors' previous study of ARB deformed AA6061 [29] where the same preheating temperature and time were used before each ARB cycle.

Unlike coarse grained metals, the UFG materials have tensile curves that peak immediately after yielding, which results in low ductility (Fig. 6(a)). The high strength and low ductility in tensile tests are the typical behaviour of UFG materials. Most of the reported UFG materials are typically several times stronger than their coarse grained counterparts which should be attributed to strain hardening (dislocation strengthening) and grain refinement hardening (grain boundary strengthening) [24]. However, at the same time, the elongation to failure is no more than a few percent [30,31]. The rapid decrement in the strain hardening rate in the ARB processed AA1050 compared to the coarse grained counterparts (Fig. 6(c)) is responsible for the early deformation instability and early fracture [21]. The changes of strain hardening rate in the current study are quite similar to that of AA1100 reported in Ref. [22], in which the strain hardening rate of 1, 4 and 8-cycle ARB processed AA1100 was shown. The strain hardening rates increase slightly with the number of ARB cycles both in the current study and in Ref. [22]. This can be attributed to the grain size effect, where the grain sizes of the higher cycle ARB processed materials are smaller. This makes the distance that dislocations need to travel before meeting grain boundaries shorter and in turn increases the resistance for further deformation. Because the grain refinement after multi-cycle ARB deformation is not as substantial as that after the first cycle ARB (Figs. 2 and 3), the increment of strain hardening rate between ARB cycles is not phenomenal.

4.3. Comparison with ECAP

ECAP process is another frequently used SPD technique to produce bulk ultrafine grained materials. Up to now, very limited studies on the comparison between ARB and ECAP process of aluminium alloys are available. To this regard, the properties of AA1050 after deformation by ECAP and ARB up to the same strain level of ~4 (4-pass ECAP and 5-cycle ARB, respectively) are compared and discussed in the following. ECAP of AA1050 was conducted using a channel die with an intersection angle of 90°. The detailed experimental procedure can be found in Ref. [32]. The properties of AA1050 processed by ECAP at room temperature in Ref. [32] were used to compare with the ARB results in the following.

Table 1 lists the grain size, average hardness, yield strength (YS) and the ultimate tensile strength (UTS) of AA1050 deformed after 4-pass ECAP and 5-cycle ARB. As can be seen from the table, the average grain size of the 5-cycle ARB processed AA1050 is about 300 nm, which is significantly smaller than the 4-pass ECAP processed AA1050. TEM micrograph of AA1050 after 4-pass ECAP processing is shown in Fig. 9. It can be seen that the grains of AA1050 after 5-cycle ARB are slightly elongated (Fig. 3(c)), while the grains after 4-pass ECAP are more equiaxed but much larger in size (Fig. 9). In fact, the average grain size after ECAP is about 600 nm which is twice of the grain size after ARB. It should be noted that the grain size values of AA1050 in the current study are slightly higher than those reported for commercial purity Al [12,18,21], and the microstructure of the AA1050 appears to be more equiaxed compared to similar alloys reported in the literature [12,18,21]. This is believed to be due to the pre-heating before rolling, which accelerates the recovery process and prevents grain refinement.

It can also be seen in Table 1 that the hardness, YS and UTS values of 5-cycle ARB processed AA1050 are considerably higher than that after 4-pass ECAP deformation. The average hardness of 4-pass ECAP processed AA1050 almost doubles the initial value whereas the value increases to about 2.5 times the initial value for the 5-cycle ARB processed sample. It can be concluded that ARB deformation is more efficient in microstructure refinement and strengthening. Note that the current ARB deformation at an elevated temperature restricts the microstructure refinement as well as strengthening. The efficiency of ARB deformation would be more obvious if the ARB process was conducted at room temperature. Cherukuri et al. [33] and Böhner et al. [20] conducted ARB and ECAP deformation on aluminium alloys up to the same accumulative strain and found that ARB processed samples had higher strength, which is consistent with the results of the present work. The difference between the ARB and ECAP processed AA1050 can be explained by the different deformation modes. The deformation mode for the ARB process is a combination of rolling at the sheet centre and shear close to the sheet surfaces, while the deformation mode for ECAP process is simple shear. It can be concluded that the combination of rolling and shear performs with a higher efficiency in grain refinement and strengthening of aluminium than simple shear.

Table 1
Comparison of AA1050 deformed by ECAP and ARB at a strain level of ~4.

	4-Pass ECAP	5-Cycle ARB
Grain size (nm)	608 ± 205	300 ± 142
Hardness (Hv)	48.8 ± 1.8	63.7 ± 2.8
YS (MPa)	111 ± 3	209 ± 1
UTS (MPa)	145 ± 4	243 ± 1

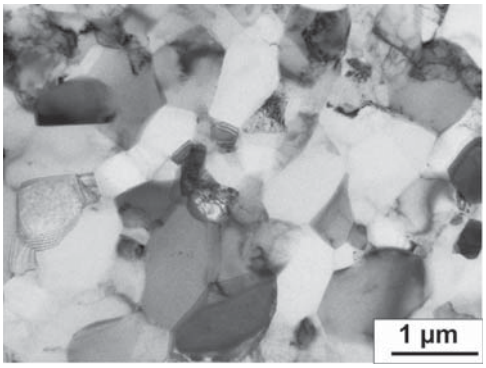

Fig. 9. TEM micrograph of AA1050 after 4-pass ECAP processing.

5. Conclusion

AA1050 sheets were processed by ARB up to five cycles in this work in order to gain a systematic understanding on the ARB process of commercial purity aluminium. Microstructure and mechanical properties of the ARB processed AA1050 were investigated in detail and they have been compared with those after ECAP at the same strain level. The results are summarised as follows:

(1) Substantial grain refinement of AA1050 has been achieved by the ARB process and the microstructure at large strains is almost uniform along the thickness direction. The misorientation between the grains becomes larger and the aspect ratio becomes smaller with the increasing number of ARB cycles. The average grain size reaches 300 nm after 5-cycle ARB from 96 μm of the initial annealed material.
(2) Two types of bond interface morphologies are observed. The type with thin band of more refined grains in between may help to improve the bond strength, but if the band width exceeds a certain level or large particles or contamination goes into the sample, the interfaces may act as origins of cracks. Bonding quality between layers gets improved by increasing rolling passes.
(3) With the number of ARB cycles, the tensile strength increases significantly and it rises up to 243 MPa after 5-cycle ARB, which is about three times the initial value. Inhomogeneous microhardness distribution along the thickness direction of ARB processed sample has been observed and the hardness values are higher near the surfaces and interfaces because of the shear strain introduced during ARB. The fracture surfaces of ARB processed AA1050 after the tensile test show typical characteristics of ductile fracture.
(4) The ARB process is more efficient in grain refinement and strengthening compared to ECAP for AA1050. The average grain size is smaller and the hardness and strength are higher for the 5-cycle ARB deformed AA1050 than that after 4-pass ECAP. These differences should be attributed to the different deformation modes, which are a combination of rolling and shear in ARB but simple shear in ECAP.

Acknowledgements

This project was supported by the Open Research Fund of Key Laboratory of High Performance Complex Manufacturing, Central South University, China, Grant no. Kfkt2013-01.The authors acknowledge the use of facilities within the UOW Electron Microscopy Centre # LE0237478 and the assistance of Dr. David Wexler. Thanks also go to Mr. Joe Abbort for his kind help of the ARB experiment.

References

[1] N.J. Petch, J. Iron Steel Inst. 174 (1953) 25–28.
[2] R. Valiev, Nat. Mater. 3 (2004) 511–516.
[3] R.Z. Valiev, R.K. Islamgaliev, I.V. Alexandrov, Prog. Mater. Sci. 45 (2000) 103–189.
[4] A.P. Zhilyaev, T.G. Langdon, Prog. Mater. Sci. 53 (2008) 893–979.
[5] Y. Saito, N. Tsuji, H. Utsunomiya, T. Sakai, R.G. Hong, Scr. Mater. 39 (1998) 1221–1227.
[6] Y. Saito, H. Utsunomiya, N. Tsuji, T. Sakai, Acta Mater. 47 (1999) 579–583.
[7] M.Y. Zhan, Y.Y. Li, W.P. Chen, W.D. Chen, J. Mater. Sci. 42 (2007) 9256–9261.
[8] R. Zhang, V.L. Acoff, Mater. Sci. Eng. A 463 (2007) 67–73.
[9] J.E. Hatch, Aluminum – Properties and Physical Metallurgy, American Society for Metals, Metals Park, Ohio, 1984.
[10] L.P. Troeger, E.A. Starke Jr., Mater. Sci. Eng. A 277 (2000) 102–113.
[11] S.H. Lee, Y. Saito, T. Sakai, H. Utsunomiya, Mater. Sci. Eng. A 325 (2002) 228–235.
[12] X. Huang, N. Tsuji, N. Hansen, Y. Minamino, Mater. Sci. Eng. A 340 (2003) 265–271.
[13] H. Pirgazi, A. Akbarzadeh, R. Petrov, L. Kestens, Mater. Sci. Eng. A 497 (2008) 132–138.
[14] S.Y. Li, F.W. Sun, H. Li, Acta Mater. 58 (2010) 1317–1331.
[15] M.Z. Quadir, A. Wolz, M. Hoffman, M. Ferry, Scr. Mater. 58 (2008) 959–962.
[16] R. Jamaati, M.R. Toroghinejad, Mater. Sci. Eng. A 527 (2010) 2320–2326.
[17] R. Jamaati, M.R. Toroghinejad, Mater. Des. 31 (2010) 4508–4513.
[18] I. Topic, H.W. Höppel, D. Staud, M. Merklein, M. Geiger, M. Göken, Adv. Eng. Mater. 10 (2008) 1101–1109.
[19] A.K. Talachi, M. Eizadjou, H.D. Manesh, K. Janghorban, Mater. Charact. 62 (2011) 12–21.
[20] A. Böhner, V. Maier, K. Durst, H.W. Höppel, M. Göken, Adv. Eng. Mater. 13 (2011) 251–255.
[21] H.-W. Kim, S.-B. Kang, N. Tsuji, Y. Minamino, Acta Mater. 53 (2005) 1737–1749.
[22] C. Kwan, Z.R. Wang, S.B. Kang, Mater. Sci. Eng. A 480 (2008) 148–159.
[23] R. Jamaati, M.R. Toroghinejad, H. Edris, Mater. Des. 54 (2014) 168–173.
[24] M. Eizadjou, H.D. Manesh, K. Janghorban, J. Alloys Compd. 474 (2009) 406–415.
[25] N. Bay, Weld. J. 62 (1983) 137s–142s.
[26] L. Su, C. Lu, A.K. Tieu, G. Deng, X. Sun, Mater. Sci. Eng. A 559 (2013) 345–351.
[27] T. Hausol, H.W. Hoppel, M. Goken, J. Mater. Sci. 45 (2010) 4733–4738.
[28] L. Li, K. Nagai, F. Yin, Sci. Technol. Adv. Mater. 9 (2008) 023001.
[29] L.H. Su, C. Lu, A.A. Gazder, A.A. Saleh, G.Y. Deng, A.K. Tieu, H.J. Li, J. Alloys Compd. 594 (2014) 12–22.
[30] R.Z. Valiev, I.V. Alexandrov, Y.T. Zhu, T.C. Lowe, J. Mater. Res. 17 (2002) 5–8.
[31] C.C. Koch, Scr. Mater. 49 (2003) 657–662.
[32] L.H. Su, C. Lu, L.Z. He, L.C. Zhang, P. Guagliardo, A.K. Tieu, S.N. Samarin, J.F. Williams, H.J. Li, Acta Mater. 60 (2012) 4218–4228.
[33] B. Cherukuri, T.S. Nedkova, R. Srinivasan, Mater. Sci. Eng. A 410–411 (2005) 394–397.